JGR Oceans

RESEARCH ARTICLE
10.1029/2023JC019723

Special Section:
Physical and biogeochemical processes affecting nutrients and the carbon cycle in mesoscale eddies of subtropical oceans

Lateral Advection of Particulate Organic Matter in the Eastern Indian Ocean

Opeyemi Kehinde[1,2], Mark Bourassa[1,2], Sven Kranz[1], Michael R. Landry[3], Thomas Kelly[1,4], and Michael R. Stukel[1,2]

[1]Department of Earth, Ocean & Atmospheric Science, Florida State University, Tallahassee, FL, USA, [2]Center for Ocean-Atmospheric Prediction Studies, Florida State University, Tallahassee, FL, USA, [3]Scripps Institution of Oceanography, University of California, San Diego, La Jolla, CA, USA, [4]College of Fisheries and Ocean Science, University of Alaska, Fairbanks, AK, USA

Abstract The Argo Abyssal Plain (AAP), south of Java and northwest of Australia in the tropical eastern Indian Ocean, is an oligotrophic region (low in chlorophyll and nutrients), downstream of the Indonesian throughflow. The processes that supply nitrogen to the AAP and support ecosystem production are unknown. Here we quantified lateral advection of particulate organic matter (POM) and the role of this advected POM in supplying new nitrogen (i.e., allochthonous nitrogen supply) to the mixed layer of the AAP using 14 yr of remotely sensed data, combined with sampling undertaken on a research cruise in February 2022. Our results indicate that the average net primary productivity of phytoplankton in this offshore oligotrophic region is 98.5 Gg C d^{-1} and that lateral advection transports 1.21 Gg C d^{-1} of particulate organic carbon (POC) into the region. We find that lateral advection of POM within the mixed layer supplies an annual average of 12% (95% C.I. = 5.2%–49%) of allochthonous "new" nitrogen supporting phytoplankton productivity, if regenerated to nutrients through microbial processes. Accounting for lateral transport in the deep euphotic zone, lateral transport supplies an average of 32% (10%–>100%) of new nitrogen, although this calculation is less certain due to inability to constrain subsurface POM fields. Our data suggest that lateral advection is a quantitatively important but not dominant source of nitrogen supporting new production. Overall, approximately half of the lateral transport is driven by transient eddies (mostly during winter) highlighting the importance of mesoscale circulation.

Plain Language Summary In most ocean regions, phytoplankton (microscopic algae that form the base of the ecosystem) are nitrogen limited. Nitrogen can enter the ecosystem through upwelling of deep waters, nitrogen fixation, or through lateral transport of particulate or dissolved organic matter which can be recycled through microbial processes. The Argo Abyssal Plain, between Indonesia and Australia, is an interesting low-nutrient study site because it is downstream of the only tropical connection between the Pacific and Indian Oceans and is also the only known spawning site for southern bluefin tuna. In this study, we combine shipboard sampling with satellite remote sensing to investigate primary production and lateral organic matter transport in the Abyssal Argo Plain. We show that lateral transport (i.e., horizontal currents that transport matter from coastal regions) is an important source, though likely not a dominant source of nitrogen, for this deepwater basin. We also show that approximately half of this lateral nitrogen supply is derived from transient eddies (i.e., rotating currents that are basically storms in the ocean that can persist for weeks or months). Substantial uncertainty remains and ascertaining how the region will respond to climatic forcing will likely require multidisciplinary programs combining shipboard sampling with synthetic modeling tools.

Key Points:

- Particulate organic carbon concentrations and net primary productivity in the Argo Abyssal Plain peak during Austral winter
- Lateral advection is quantitatively important, but not the dominant source of nitrogen supporting phytoplankton new production
- Remote-sensing results suggest that most of the laterally advected organic matter in this region is eddy-driven

Correspondence to:
O. Kehinde,
opeyemi.kehinde891@gmail.com

Citation:
Kehinde, O., Bourassa, M., Kranz, S., Landry, M. R., Kelly, T., & Stukel, M. R. (2023). Lateral advection of particulate organic matter in the eastern Indian Ocean. *Journal of Geophysical Research: Oceans*, *128*, e2023JC019723. https://doi.org/10.1029/2023JC019723

Received 7 FEB 2023
Accepted 26 APR 2023

Author Contributions:
Conceptualization: Mark Bourassa
Data curation: Opeyemi Kehinde, Michael R. Landry, Thomas Kelly
Formal analysis: Opeyemi Kehinde
Funding acquisition: Mark Bourassa, Sven Kranz, Michael R. Landry, Michael R. Stukel
Investigation: Opeyemi Kehinde
Methodology: Opeyemi Kehinde, Mark Bourassa, Michael R. Stukel
Project Administration: Opeyemi Kehinde, Mark Bourassa, Michael R. Stukel
Resources: Opeyemi Kehinde, Michael R. Stukel
Software: Opeyemi Kehinde, Thomas Kelly, Michael R. Stukel
Supervision: Mark Bourassa, Michael R. Stukel

1. Introduction

Most open ocean pelagic ecosystems are nitrogen-limited (Duce et al., 2008), with continuous or episodic nitrogen supply crucial for sustaining system productivity. Open-ocean waters rely on new production to balance nitrogen lost through sinking, subducted organic matter, exploited stocks or migratory higher trophic levels. New production refers to phytoplankton organic matter produced based on nitrogen coming from outside of an ecosystem (as opposed to nutrients remineralized in the euphotic zone), with the primary sources of new production (nitrogen fixation, upwelling, and lateral advection) typically accounting for ~10% of net primary productivity (NPP) in oligotrophic waters (Eppley & Peterson, 1979; Lipschultz, 2001; Yingling et al., 2022).

Validation: Sven Kranz
Writing – original draft: Opeyemi Kehinde
Writing – review & editing: Mark Bourassa, Sven Kranz, Michael R. Landry, Thomas Kelly, Michael R. Stukel

Advective processes reshape biogeochemical patterns in the open-ocean pelagic when cross-shore currents transport high-nutrient and high-biomass (i.e., high particulate organic carbon, POC) water from the coast to offshore areas through cold filaments, offshore propagating mesoscales eddies and Ekman currents (Amos et al., 2019; Chabert et al., 2021; Nagai et al., 2015). Such horizontal transport can decouple net community production and new production from export production at meso- and larger scales (Estapa et al., 2015; Kranz et al., 2020; Plattner et al., 2005). The offshore phytoplankton community can utilize the allochthonous organic nitrogen transported from the coast either after that organic nitrogen is remineralized to NH_4^+ by zooplankton and the microbial loop (Azam et al., 1983; Steinberg & Landry, 2017) or, in some cases, when dissolved organic molecules are directly taken up through cellular transporters (Granéli et al., 1999; Yelton et al., 2016) or when particulate prey is consumed by mixotrophs (Stoecker et al., 2017). In either case, this laterally transported nitrogen can be fixed into phytoplankton biomass, which can be consumed by zooplankton, and in turn, by higher trophic level organisms like fish. For these reasons, frontal eddies sourced from continental shelf waters have been hypothesized to be important fish nursery habitat (Suthers et al., 2023).

The mixed layer above the Argo Abyssal Plain (surface area ~340,000 km, hereafter referred to as Argo Basin) in the eastern tropical Indian Ocean is a poorly studied region downstream of the Indonesian throughflow (ITF), which is the only tropical connection between Pacific and Indian Ocean waters (Figure 1). ITF enters the Indian Ocean through three routes which are: the Lombok straits, Timor passage, and Omboi Straits (Figure 1; Ayers et al., 2014; Valsala & Ikeda, 2007). The ITF, largely affected, seasonally and interannually, by remote forcing from planetary waves and monsoon winds (Ayers et al., 2014), transports large amounts of warm water through the Indonesian Seas into the Indian Ocean (Muhling et al., 2017; Tomczak & Godfrey, 2003). ITF is part of the upper branch of the global heat conveyor belt, and thus important for balancing heat, salt, and nutrient budgets in the oceans. Complex and temporally variable currents and other processes re-distribute water masses (hence nutrients and organisms) throughout this specific region with four major currents, the Indonesian throughflow, the Leeuwin Current, the Sectoral Equatorial Current, and the Eastern Gyral Current acting upon it (Figure 1). Strong mesoscale activity (Nieblas et al., 2014) additionally affects biogeochemistry in this region. Due to seasonally reversing southeast (May–October) and northwest (January–March) monsoonal winds, coastal and open ocean upwelling can introduce nutrients to the surface ocean and support phytoplankton production. Despite the region being characterized by low chlorophyll concentration and presumably low plankton biomass, the Argo Basin has special ecological and economic importance as it is the only known spawning site for southern bluefin tuna (SBT), a species with circumglobal adult populations.

A comparable ecosystem for the ITF/Argo Basin region is the offshore Gulf of Mexico (GoM). Both systems are warm, stratified, nutrient-poor, deep-water basins in close proximity to more productive coastal margins, and both are rich in high-kinetic-energy mesoscale features. Coincidentally, both are major spawning and rearing grounds for larvae of bluefin tuna (Atlantic Bluefin tuna in the GoM; Rooker et al., 2007), whose recruitment success depends on the ability to grow rapidly and minimize losses to predators in a very low food environment (Gerard et al., 2022; Shiroza et al., 2022; Shropshire et al., 2020; Yingling et al., 2022). In the GoM, Kelly et al. (2021) showed that laterally advected organic matter is sufficient to support more than 90% of nitrogen export (equivalent to new production) in the oligotrophic ocean waters, while upwelling and nitrogen fixation account for little of the nitrogen supply. Based on these results, we hypothesized that lateral advection of organic matter contributes substantially to the new nutrients that sustain productivity in the Argo Basin/ITF region. It was further surmised that much of this lateral advection may be the direct result of eddies (e.g., closed circular currents typically 100–300 km in diameter) and other mesoscale features based on the demonstrated importance of such currents in the eastern tropical Indian Ocean (Waite et al., 2016). We tested these hypotheses using remote sensing observations (through the combination of POC, surface currents, and mixed later depth data as outlined in Section 2.5), validation of the remotely sensed data using direct in situ measurements (Section 3.1) and lastly, quantification of the contribution of mesoscale features like eddies to cross-shore transport of POC (Section 3.4).

2. Data and Methods

2.1. Particulate Organic Carbon

2.1.1. Satellite-Derived POC

POC concentrations were estimated from remote observations of reflectance from the Moderate Resolution Imaging Spectrometer (MODIS) sensor operating on both the NASA Terra and Aqua spacecraft at a high resolution of 4 km and a scanning frequency of 2 days, using the algorithm described by Stramski et al. (2008). This algorithm

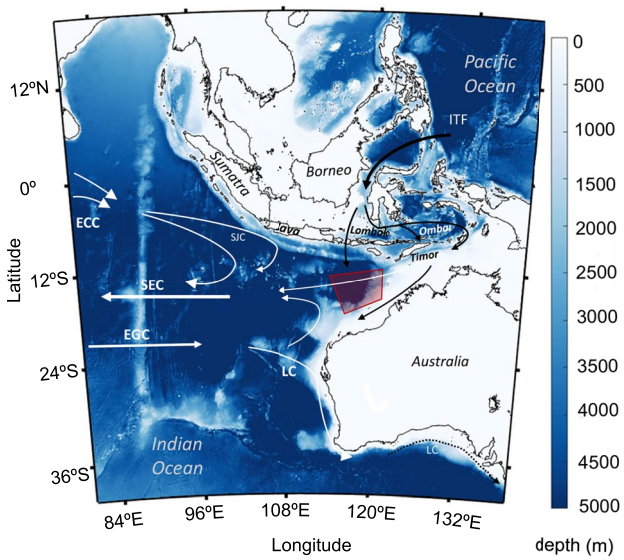

Figure 1. A bathymetric map showing depth (in meters) and the Argo Basin (red quadrilateral) which is our study region. Thick arrows indicate major surface currents: Equatorial Gyral Current (EGC), Indian throughflow (ITF), Leeuwin Current (LC), and Sectorial Equatorial Current (SEC).

(Equation 1) uses an empirical relationship derived from in situ measurements of POC and blue-to-green band ratios of remote sensing reflectances (R_{rs}) to determine the concentration of POC in mg/m^3.1

$$\mathrm{POC} = a \times \left(\frac{\mathrm{Rrs}(443)}{\mathrm{Rrs}(555)}\right)^{b} \quad (1)$$

where $a = 203.2$, $b = -1.034$, Rrs(443) is the 438–448 nm band in the blue region and Rrs(555) is the 546–556 nm band in the green region. Evers-King et al. (2017) showed that this algorithm performed well across different water types.

Aqua satellite data were obtained for the years 2003–2016 in 8-day composites, from the NASA Ocean Color website (https://oceancolor.gsfc.nasa.gov/l3/) and linearly interpolated to calculate POC fluxes through the boundary of the study region (Figure 2). Cloud coverage reduced the usable data frequency and introduced spatial and temporal biases. To avoid errors introduced through excessive spatial interpolation on cloudy days, we used only satellite images with more than 80% data coverage of our study area in the 8-day averaged POC data.

2.1.2. In Situ POC Data

To validate the remotely sensed POC data, in situ measurements were taken during the BLOOFINZ-IO cruise (Bluefin Larvae in Oligotrophic Ocean Foodwebs Investigations of Nutrients to Zooplankton in the Indian Ocean), conducted from January 2022 to March 2022 on *R/V Roger Revelle.* We sampled conditions that ranged from high-biomass coastal regions to oligotrophic offshore waters in the Argo Basin northwest of Australia, including crossings of mesoscale eddies. The cruise consisted of three distinct components: (a) transits when only underway surface sampling was possible, (b) transects which included CTD-Niskin rosette hydrocasts allowing us to collect depth profiles of POC across a large area, and (c) quasi-Lagrangian experiments conducted over ∼4-day (Gerard et al., 2022; Landry et al., 2009), during which CTD deployments were made twice daily at 06:00 and 22:00 local to collect water column samples of POC. During transits, we collected samples approximately hourly (∼2 km distance between samples) directly from the ship's uncontaminated flowthrough seawater system (nominal depth = 5 m). During transects, water budgets were limited so we only collected samples from four depths (typically ∼5, ∼40, the deep chlorophyll maximum depth, and ∼100 m). During quasi-Lagrangian experiments, we typically sampled from ∼2 casts per day. One cast sampled six depths spanning the euphotic zone. The second cast typically sampled 12 depths from the surface to a depth of 220 m. We sampled 4L into polyethylene sample bottles (reduced volumes were occasionally used in high biomass regions). Samples were filtered onto pre-combusted glass fiber filters (GF/F), wrapped in pre-combusted aluminum foil, and dried at 40°C for 24 hr before being stored for later analysis on land. On land, samples were fumed with HCl in a desiccator for 24 hr to remove inorganic carbon. Samples were analyzed with an isotope ratio mass spectrometer (CE Instruments NC2500 EA coupled to a Thermo Scientific Delta Plus XP iRMS) at the University of California Santa Cruz to quantify POC (as well as isotopes, although isotopes are not presented in this study). Typical precision is 2.5 µg C.

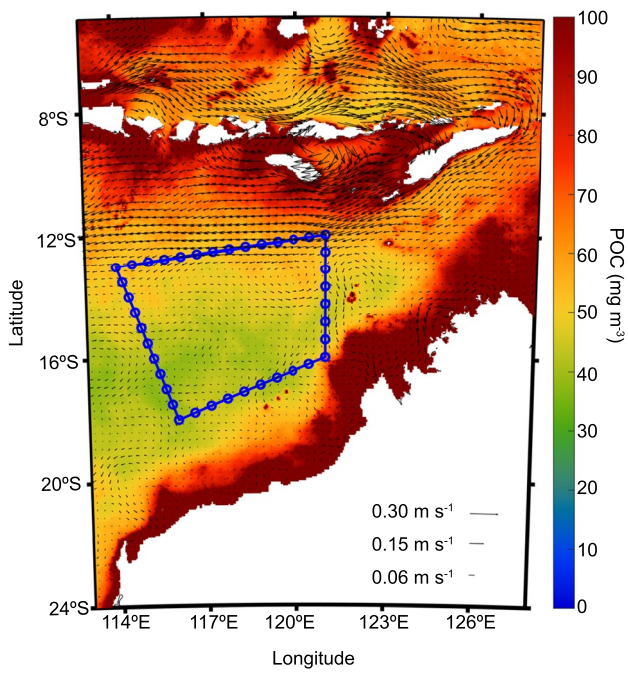

Figure 2. Average particulate organic carbon (POC) and current data for 2003 with our study region bounded by four coordinates: (13°S 114°E) (18°S 116°E) (16°S 121°E) (12°S 121°E). The blue circles indicate the interpolated points, and the thick black quadrilateral represents our study region.

2.2. Net Primary Productivity

NPP rates were estimated from the vertically generalized production model (VGPM), a chlorophyll-based model proposed by Behrenfield and

Falkowski (1997), as a function of chlorophyll, photosynthetic efficiency, and light availability. Similar to POC, NPP data were obtained in 8-day composites and cloudy 8-day periods were ignored. To estimate spatial trends in NPP, we integrated NPP across the study region (Figure 1) and multiplied each grid cell area by the amount of NPP in that grid, then summed the results for each grid cell using the equation below.

$$\text{Net primary productivity} = \sum^{n}(\text{area} \times \text{NPP}) \tag{2}$$

for which:

area, is the area of each grid cell in m^2, while NPP is the net primary productivity in each grid cell in mg C m^{-2} d^{-1}, and n is the number of grid cells.

2.3. Surface Currents

POC transport analyses were based on sea surface current data provided by the European Space Agency, which encompasses a nearly 24 yr period from January 1993 to May 2017. We, however, only used data starting January 2003 through December 2016 (14 yr) to match the temporal range of the MODIS data (May 2002 to December 2021). The spatial resolution is 0.1° and the temporal resolution is 3 hr for the whole data set. This GlobCurrent product is a combined estimate of the geostrophic and Ekman components—based on altimetry, gravimetry, and in situ data from Argo float, drifting buoys, and CTD casts—that is valid at the surface and at 15-m depth (Globcurrent.org, Rio et al., 2014). Drifters moving roughly with the 15-m current were used as a daily in situ reference. This product is most suitable for open-ocean waters like our study region (Cancet et al., 2019), and the estimation approach is similar to that used for the Ocean Surface Current Analysis Real Time (Bonjean & Lagerloef, 2002) and Geostrophic and Ekman Current Observatory (Sudre et al., 2013) currents products (Rio et al., 2014).

The northward current (V) and the eastward current (U) were averaged over 8-day intervals (to match POC temporal resolution) and interpolated to the boundary of the domain to estimate POC flux through the boundary. Velocities were rotated using a rotation matrix such that all positive U' components are inwardly perpendicular to the domain, showing influx. In contrast, the V' component is the velocity parallel to the domain.

2.4. Mixed Layer Depth Data

To estimate total flux in the mixed layer, we incorporated the Atlas mixed layer depth (MLD) products by Monterey and Levitus (1997), which uses standard criteria by the National Oceanographic Data Center (NOAA). This product is a climatological monthly mean of mixed layer depths for the world ocean from the NOAA National Center Environmental Information (NCEI). This product was computed based on three criteria: a temperature change from the ocean surface of 0.5°C, a density change from the ocean surface of 0.125 (sigma units), and a variable density change from the ocean surface corresponding to a temperature change of 0.5°C (NOAA Atlas). These monthly data were interpolated into 8-day intervals to match the rest of our satellite data.

2.5. Remote-Sensing Estimates of POC Transport

Remotely sensed POC data were combined with the remote sensing circulation product GlobCurrent to infer lateral flux of POC across the study region boundaries. A grid was drawn around the region and the POC flux data were interpolated over evenly spaced points (~61-km segments) along the edge of this region (Figure 2). The POC flux at the midpoint of each 61-km segment of the POC was calculated by multiplying the interpolated POC by the perpendicular velocity and the distance between each interpolated point (Equations 3 and 4).

$$\text{Flux} = \int_{d}\int_{0}^{\text{MLD}} \text{POC} \times U' dz dl \tag{3}$$

$$\text{Net Flux} = \oint_{d}\int_{0}^{\text{MLD}} \text{POC} \times U' dz dl \tag{4}$$

for which:

POC (in mg C m^{-3}) represents interpolated POC, U' (in m s^{-1}) represents perpendicular velocity (positive inward), d (in m) is the distance between each interpolated point and MLD (in m) represents mixed layer depth. The sum of the fluxes in Equation 3 explains the flux of POC into (if positive) or out of (if negative) the region as shown in Equation 4.

2.6. Organic Matter Flux Associated With the Mean Flow and Mesoscale Features

To determine the transport of POC across the study region's boundaries associated with mean flow, transient mesoscale features, and persistent eddies, we used Equation 5, from Lorenz (1967). Here, transient eddies are defined as propagating eddies, that is, eddies that move across the domain while persistent eddies occupy roughly the same location throughout the study period. Both persistent eddies and mean flow have spatial patterns that persist over time, but mean flow represents the space and time-averaged flow, whereas persistent eddies have a smaller spatial structure. Lorenz's equations can be used to determine transport by each of these features. The first term in Equation 5 is the longitudinally and temporally averaged transport of POC $\left(\left[\overline{PU}\right]\right)$. The second term $\left(\left[\overline{P}\right]\left[\overline{U}\right]\right)$ is transport due to mean flow and mean POC. The third term $\left(\left[\overline{P'U'}\right]\right)$ is the transport associated with transient POC and currents, and the last term $\left(\left[\overline{P*}\,\overline{U*}\right]\right)$ is associated with transport by persistent eddies. The last two terms can be combined to indicate transport by eddies and other mesoscale features.

$$\left[\overline{PU}\right] = \left[\overline{P}\right]\left[\overline{U}\right] + \left[\overline{P'U'}\right] + \left[\overline{P*}\,\overline{U*}\right] \tag{5}$$

in which bars represent averaging in time, prime denotes the difference from a temporal average, square brackets indicate a spatial average, and asterisks are the difference from a spatial average.

2.7. Nonparametric Uncertainty Propagation

Because data were not normally distributed, we used a nonparametric Monte Carlo approach to quantify uncertainty in the proportion of new production supported by lateral advection of particulate organic matter in the mixed layer. Uncertainty in annual POC lateral transport was determined from the variability in annual averages calculated from Equation 4 using a bootstrapping approach (i.e., in each Monte Carlo simulation, we randomly sampled with replacement from the 14 yr with available remotely sensed data). Uncertainty in annual average NPP was determined the same way. We modeled the Argo Basin f-ratio (i.e., ratio of new production to total production) as a beta distribution (because it can only take values between 0 and 1) with $\alpha = 3.5$ and $\beta = 31.5$ (equating to mean value of 0.1 and a standard deviation of 0.05, which we take to be representative of oligotrophic regions). The fraction of new production supported by mixed layer lateral transport was calculated as:

$$\text{Fraction Lateral}_{\text{MLD}} = \frac{\text{Net Flux}}{\text{NPP} \times \text{fratio}} \tag{6}$$

where Net Flux is calculated from Equation 4. Equation 6 implicitly assumes that the C:N ratio of POM entering the ecosystem is similar to the C:N ratio of new phytoplankton production. We note that Equation 6 neglects lateral transport of organic matter occurring in the euphotic zone beneath the mixed layer. If we assume that (a) horizontal currents in the mixed layer are similar to horizontal currents deeper in the euphotic zone and (b) that the ratio of POC concentration in the deep euphotic zone to POC concentration in the mixed layer measured on our cruise is representative of the region, then we can estimate the lateral transport of POC throughout the euphotic zone as:

$$\text{Fraction Lateral}_{\text{Eup}} = \frac{\text{Net Flux}}{\text{NPP} \times \text{fratio}} \times \frac{\text{EUD}}{\text{MLD}} \times \frac{\text{POC}_{\text{Eup}}}{\text{POC}_{\text{ML}}} \tag{7}$$

where EUD is the euphotic zone depth (defined conservatively as the 1% light level, with uncertainty derived from differences between multiple CTD hydrocasts on the BLOOFINZ-IO cruise), MLD is the mixed layer depth (with uncertainty derived from the MLD product), and POC_{Eup} and POC_{ML} are the average POC concentrations in the euphotic zone and mixed layer, respectively (with uncertainty derived from multiple profiles on

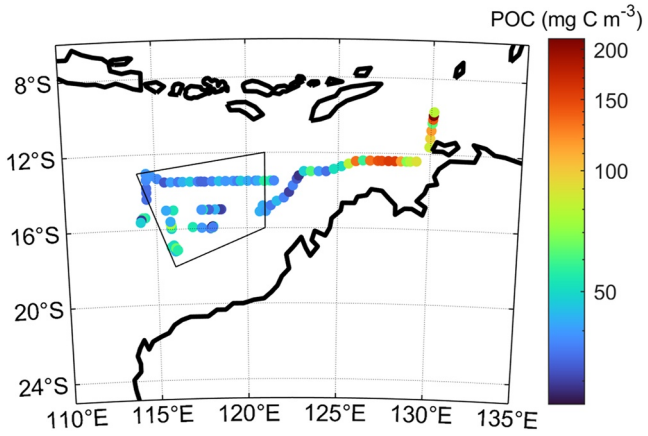

Figure 3. Surface particulate organic carbon (POC) concentrations (mg C m^{-3}) measured on the BLOOFINZ-IO cruise in January–March 2022. Black quadrilateral shows our Argo Basin control volume.

the cruise). We conducted 10,000 Monte Carlo simulations and used these to determine asymmetric 95% confidence limits for $FractionLateral_{MLD}$ and $FractionLateral_{Eup}$.

3. Results and Discussion

3.1. In Situ POC and Comparison to Satellite POC

Within the study area's control volume (i.e., the quadrilateral in Figures 2 and 3), surface POC concentrations measured from February to March of 2022 varied from 30 to 76 mg C m^{-3}, with most values ranging from 35 to 50 mg C m^{-3} (Figure 3). On the shelf break near Australia, however, POC concentrations were occasionally much higher, reaching 160–220 mg C m^{-3}. POC concentrations did not show much variability with depth in the upper 100 m (Figure 4), typically increasing from the surface until the depth of the chlorophyll maximum (which was typically at ~75 m depth, Figure 4) and then declining beneath the chlorophyll maximum. Notably, the euphotic zone (average depth = 80 m, if defined by the 1% light level; depth = 119 m, if defined by the 0.1% light level) was substantially deeper than the mixed layer, which varied from 18 to 58 m throughout the year in the Argo Basin (Figure 5).

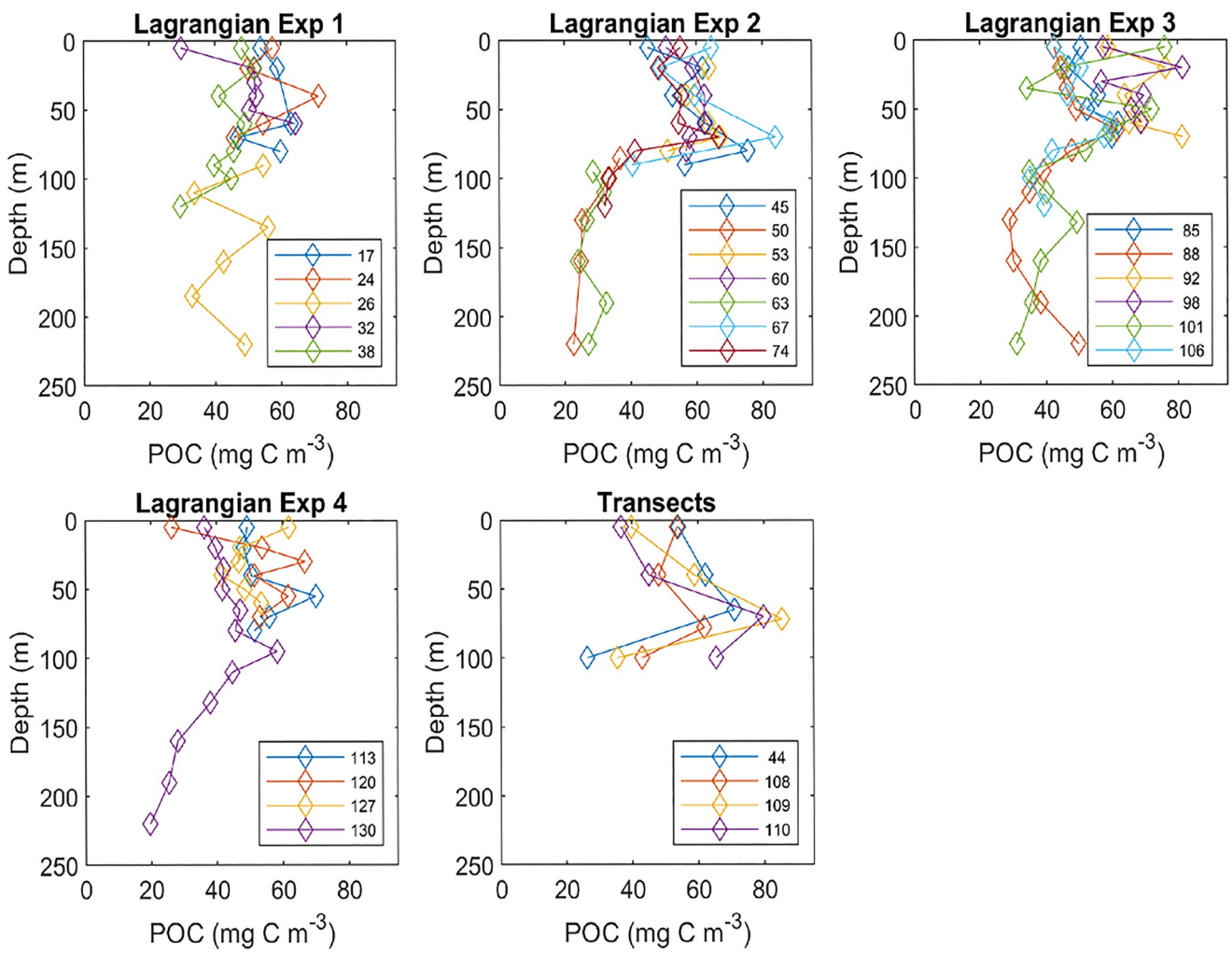

Figure 4. Vertical profiles of particulate organic carbon (POC) measured on the BLOOFINZ-IO cruise. Color indicates cast number.

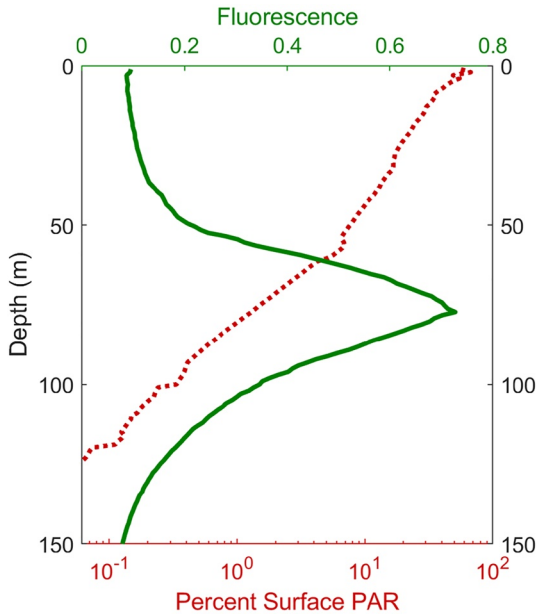

Figure 5. Average fluorescence (solid green line) and photosynthetically active radiation (dotted red line) profiles in the study region as measured on the BLOOFINZ-IO cruise.

Figure 6 shows the comparison of in situ and satellite measurements of POC for our region. We matched in situ surface measurements (≤10 m) to daily satellite data based on the closest cloud-free satellite pixel (Figure 6) and retrieved a total of 49 data points. The root mean squared deviation, or root mean squared error (RMSE), was used to assess the uncertainty in these data. The average relative percentage difference (RPD) provides the general degree of agreement between both measurements. The RMSE, the average absolute error (AAE), and the average error (AE, bias) are measures of the size of divergence or disagreements between the satellite-derived POC and in situ POC measurements. Values close to zero signify a close match. R^2 shows how well the satellite data explains the observed data; the closer the R^2 value is to 1, the better the match. The RMSE of the satellite matchups (using closest data within 200 km or less) was 26.7 mg C m^{-3}, while the AAE was 15.9 mg C m^{-3}, RPD was −15%, and the bias (AE) was −12.6 mg C m^{-3} (Table 1). The determination coefficient (R^2) value was 0.6 and the slope of the linear regression was approximately 0.57, while the intercept was 11.3 mg m^{-3}. Furthermore, the RMSE, AAE, RPD, and bias are 26.7, 15.9, −15, and −12.6 respectively. The RMSE of the satellite matchups (using closest data within 125 km or less) was 14.1 mg C m^{-3}, while the AAE was 11.1 mg C m^{-3}, RPD was −8.7%, and the bias (AE) was −8.1 mg C m^{-3} (Table 1). The determination coefficient (R^2) value was 0.9 and the slope of the linear regression was approximately 0.8, while the intercept was 1.4 mg m^{-3}. Furthermore, the RMSE, AAE, RPD, and bias are 14.1, 11.1, −8.7, and −8.1 respectively. Table 2 summarizes the statistical results of these data and the equations used. Comparison of these data shows that the two sets of observations are on similar scales with good matches for typical values, although the satellite data occasionally underestimates POC when the concentration was high (above 120 mg m^{-3}). This comparison shows no indication of a large problem in satellite calibration for the region, especially when considering that the satellite remote sensing product explicitly averages out submesoscale variability (providing an 8-day, 4-km × 4-km average of mixed layer concentrations) while our in situ measurements were point measurements from a 4-L bottle and not always perfectly collocated with satellite measurements.

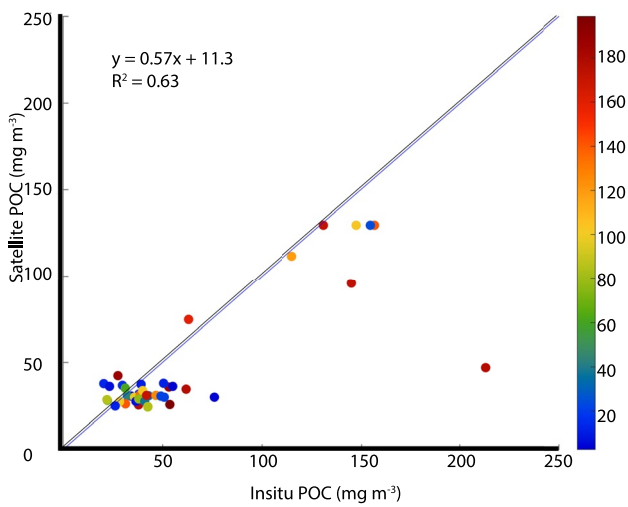

Figure 6. Comparison of in situ and satellite-derived particulate organic carbon (POC) estimates. Data represent matchups for the concurrent satellite and field measurements taken during the BLOOFINZ research project in the eastern Indian Ocean. The blue solid line shows the 1:1 relationship. The in situ data spatial locations are depicted in Figure 3. The color on the right *Y*-axis shows how far a matched satellite observation is (in km), from the in situ measurement. The corresponding error statistics are shown in Table 1.

3.2. POC Flux

An annual quantitative comparison of the Net Flux through the boundary shows that an average POC amount of 1.21 Gg C d^{-1} flows into this region (Figure 7a). The absolute magnitude of net POC flux was highest during the winter, although Net Flux varied primarily into (e.g., 2007) and out (e.g., much of 2012) of the region as shown in Figure 7a. This suggests that some factors are triggering high POC flux every winter. These factors could include seasonal reversing winds (monsoons), changes in rain rate modifying river outflow, ocean eddies, and currents. The Southwest Monsoon which usually occurs during this period brings winds that trigger the formation of ocean eddies which trap and transport nutrients (and biomass) into and out of the region. The years 2007 and 2010 had a POC influx of over 10 Gg C d^{-1}, in July during the austral winter, while a net loss of POC from the study region occurred in winter 2004. However, these fluxes were quite variable throughout the austral winter. In contrast, austral summer, autumn, and spring demonstrated lower POC fluxes and low year to year variability in these seasons, although we have fewer data during austral summer due to cloud cover (Figure 7a). The 14-yr satellite record enables us to compare interannual variability in POC flux in the Argo Basin, with annual average POC flux ranging from 0.23 to 3.20 Gg C d^{-1} (Figure 9).

POC fluxes were averaged at 8-day intervals through the study period to investigate the seasonal climatological trend (Figure 8a). The resulting POC influx

Table 1
Summary of the Statistics That Is, the Root Mean Square Deviation (RMSD), Average Relative Percentage Difference (RPD), Root Mean Square Error (RMSE), the Average Absolute Error (AAE), Average Error (AE) and R^2 Coefficient for the POC Concentrations (mg m^{-3}) Compared in Figure 6, Where "P" Are the Satellite Data and "O" Are the In Situ Data

Statistic	Result (based on match ups less than 200 km)	Result (based on match ups less than 125 km)	Equation
RMSE	26.7	14.1	$\mathrm{RSME} = \sqrt{\frac{\sum_{i=1}^{n}(P_i - O_i)^2}{n}}$
RPD	−15.0	−8.7	$\mathrm{RPD} = \frac{i}{n}\sum_{i=1}^{n}\frac{P_i - O_i}{O_i} * 100\%$
AAE	15.9	11.1	$\mathrm{AAE} = \frac{\sum_{i=1}^{n}\lvert P_i - O_i\rvert}{n}$
AE (bias)	−12.6	−8.1	$\mathrm{AE} = \frac{\sum_{i=1}^{n}(P_i - O_i)}{n} = \overline{P} - \overline{O}$
R^2	0.6	0.9	$R^2 = \left[\frac{\sum_{i=1}^{n}\left(P_i - \overline{P}_i\right)\left(O_i - \overline{O}_i\right)}{\sum_{i=1}^{n}\left(P_i - \overline{P}_i\right)^2\left(O_i - \overline{O}_i\right)^2}\right]^2$

is highest in July (austral winter; +3.08 Gg C d^{-1}) while the greatest outflow of −0.32 Gg C d^{-1} occurs in October (austral spring). POC flux gradually increases to +2.45 Gg C d^{-1} by April (austral autumn) and declines again around September, from late winter to spring (Figure 8a). However, the flux sharply decreased to +0.7 Gg C d^{-1} in early August. The POC flux during summer, autumn, and spring are consistently low with a small range, compared to winter when there is highest monthly mean POC flux by July. The average POC flux during the austral summer (December to February), austral autumn (March–May), austral winter (June–August), and austral spring (September–November) were 0.55, 1.25, 1.79, and 0.50 Gg C d^{-1}, respectively.

3.3. Net Primary Productivity

Our results indicate that the average NPP of this offshore oligotrophic region is 98.5 Gg C d^{-1} (Figure 7b). NPP is lower during austral autumn and spring, and higher during austral winter. We found a weak linear correlation of 0.30 between POC flux and NPP, which suggests that laterally advected POC is not the main driver of productivity in the region. Climatologically, we observed the highest NPP of 130 Gg C d^{-1} from late July to early August (Figure 8b), while the least productive period is March (70 Gg C d^{-1}) toward the end of the austral summer season, as productivity gradually increases and decreases around autumn and spring respectively.

The NPP of the Argo Basin in the eastern Indian Ocean was highest in 2004 (112.0 Gg C d^{-1}) and lowest in 2016 (78.4 Gg C d^{-1}). The average NPP during the austral summer (December–February), austral autumn (March–May), austral winter (June–August), and austral spring (September–November) was 74.1, 73.8, 121.3, 96.5 Gg C d^{-1}, respectively (Figure 9a).

If we assume that the Argo Basin has an *f*-ratio of 10% (i.e., new production supports 10% of NPP), then new production (on a carbon basis) is on the order of 10 Gg C d^{-1} and 12% (i.e., 1.21 Gg C d^{-1}) of new production is supported by lateral advection of organic matter within the mixed layer, although this value showed substantial uncertainty with 95% confidence intervals of 5.2%–49% of new production supported by mixed layer lateral transport. This estimate only accounts for POC transport within the mixed layer since remote sensing products cannot estimate subsurface POC concentrations. Our in situ measurements indicate that the euphotic zone is usually substantially deeper than the mixed layer and that POC concentrations are actually higher in the deep euphotic zone (near the deep chlorophyll maximum) than in the mixed layer (Figure 4). If we assume that horizontal currents are similar throughout the euphotic zone, the total euphotic zone lateral transport of POC from Equation 7 supports 32% of new production (with 95% C.I. of 10 - >100%). This value should be approached with some caution, however, due to our inability to constrain subsurface processes from satellite remote sensing products.

Table 2
The Amount of Particulate Organic Carbon (POC) in Gg C d^{-1} Transported Through Mean Flow, Transient Eddies, and Persistent Eddies Through the Four Boundaries of Our Study Region

	$\left[\overline{P}\right]\left[\overline{U}\right]$	$\left[\overline{P'U'}\right]$	$[\,\overline{P} * \overline{U} *]$
	Transport by mean flow	Transport by transient eddies	Transport by persistent eddies
Western boundary	−0.24	+0.10	−0.04
Southern boundary	−0.60	+0.05	+0.00
Eastern boundary	+1.00	+0.18	+0.11
Northern boundary	+0.12	+0.14	−0.01
Total (Gg C)	**+0.30**	**+0.46**	**+0.06**

We also calculated the seasonal contribution of lateral advection (mixed layer only) to new production and found that lateral advection contributes 7% of new production during the austral summer, 16% during the austral autumn, 14% during the austral winter and 5% during the austral spring (Figure 8). Total euphotic zone lateral transport would, of course, have been substantially greater. Annual average contributions of mixed-layer POC flux to new production in this region ranged from 2% to 29%. The highest contributions were observed in 2007 (29%), 2010 (24%), and 2016 (16%), while the lowest contribution (2%) was observed in 2012. In 2004, 2009, and 2011, similarly low contributions of 4%, 5%, and 5% were observed.

3.4. Mean Transport and Eddies

Using Equation 5, we determined the relative importance of mean flow, persistent eddies, and transient eddies in driving lateral transport of POC. Mean flow (integrated over the average mixed-layer depth of 30 m and assuming

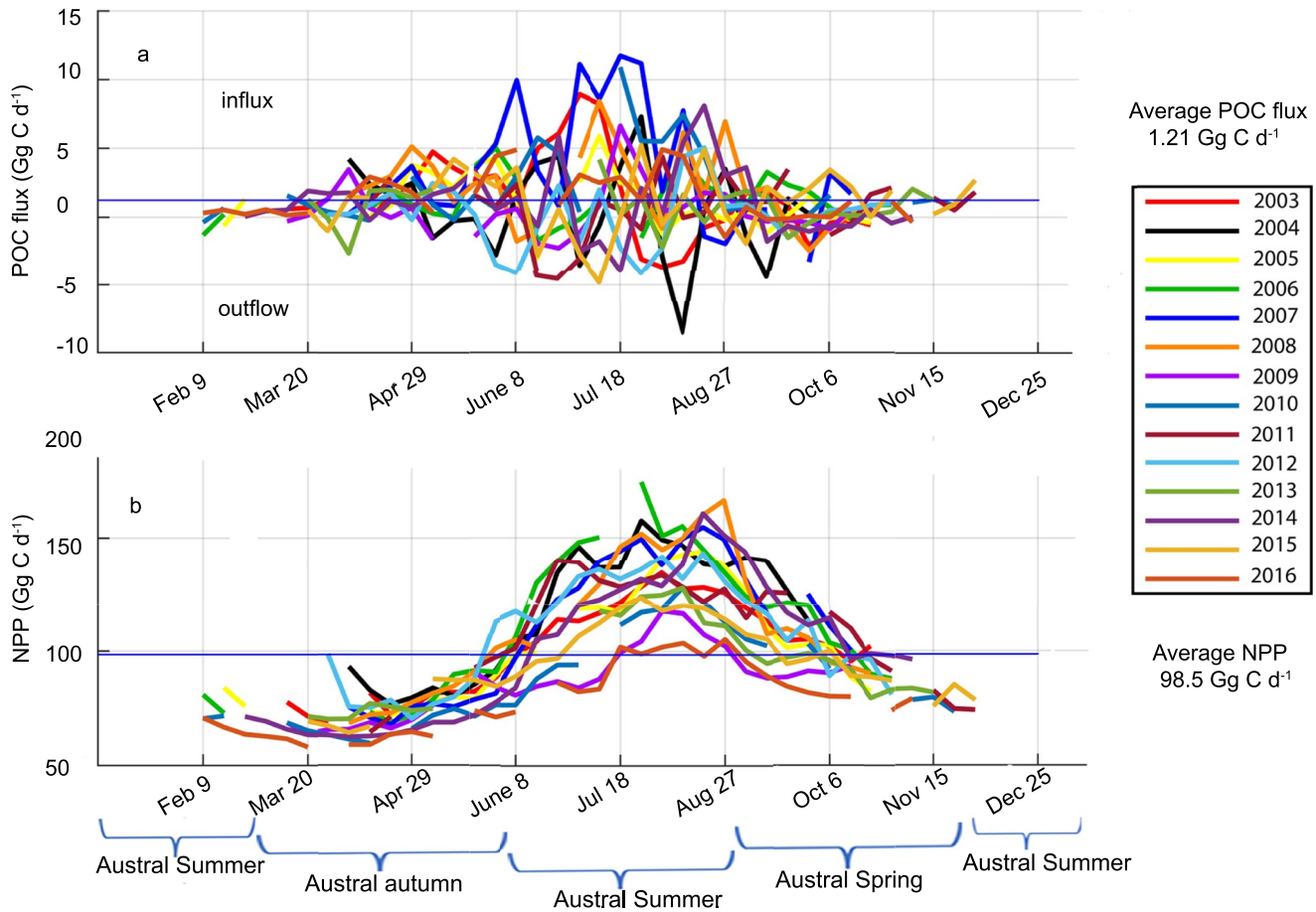

Figure 7. (a) Particulate organic carbon (POC) flux in the study region, estimated from 8-day composites of POC, surface currents, and mixed layer depths (2003–2016). (b) Annual net primary productivity of the region. The horizontal lines represent the average for each data set.

that remotely sensed POC and currents apply to this layer) was responsible for an average of 0.3 Gg C d^{-1}, while transient eddies transported 0.4 Gg C d^{-1} and persistent eddies transported 0.06 Gg C d^{-1} (Table 2, Figure 10). Mean flow transport was primarily in through the eastern boundary and out through the western and southern boundaries. Transient eddies, by contrast, had positive inflow through all boundaries, with greatest flow through the eastern boundary. The eastern and northern boundaries face the pathway through which the ITF transports Pacific Ocean water into the Indian Ocean, and they are also surrounded by productive coastal waters, accounting for their importance to mean flow transport.

3.5. Lateral Transport and the Epipelagic Ecosystem

The Argo Basin region downstream of the ITF is a classic example of a tropical, oligotrophic ecosystem with relatively low productivity and a deep-chlorophyll maximum. Oligotrophic ecosystems are characterized by low nutrient and chlorophyll concentrations, and low plankton biomass, yet, despite prey scarcity, these regions serve as the nursery sites for many fish species (Muhling et al., 2017). A comparative ecosystem for the Argo Basin is the open ocean GoM, that is also characterized as oligotrophic with a deep nitracline and low productivity (Gerard et al., 2022; Yingling et al., 2022), while being spatially close to its productive coastal waters (Barkan et al., 2017; Fennel & Laurent, 2018; Kelly et al., 2021). A previous study (Kelly et al., 2021) showed that the upper euphotic zone of the GoM open waters is supported primarily by lateral advection of organic matter, compared to locally upwelled nutrients and N_2-fixation. Here, we hypothesized that similar processes might be dominant in the offshore eastern Indian Ocean. In contrast to the findings of Kelly et al. (2021), our results indicate that lateral advection contributes a smaller fraction of the nitrogen supporting the ecosystem (12% mean, 4.2%–49% at the 95% C.I. if only including mixed layer transport, 32% mean, 10 - >100% if integrating over

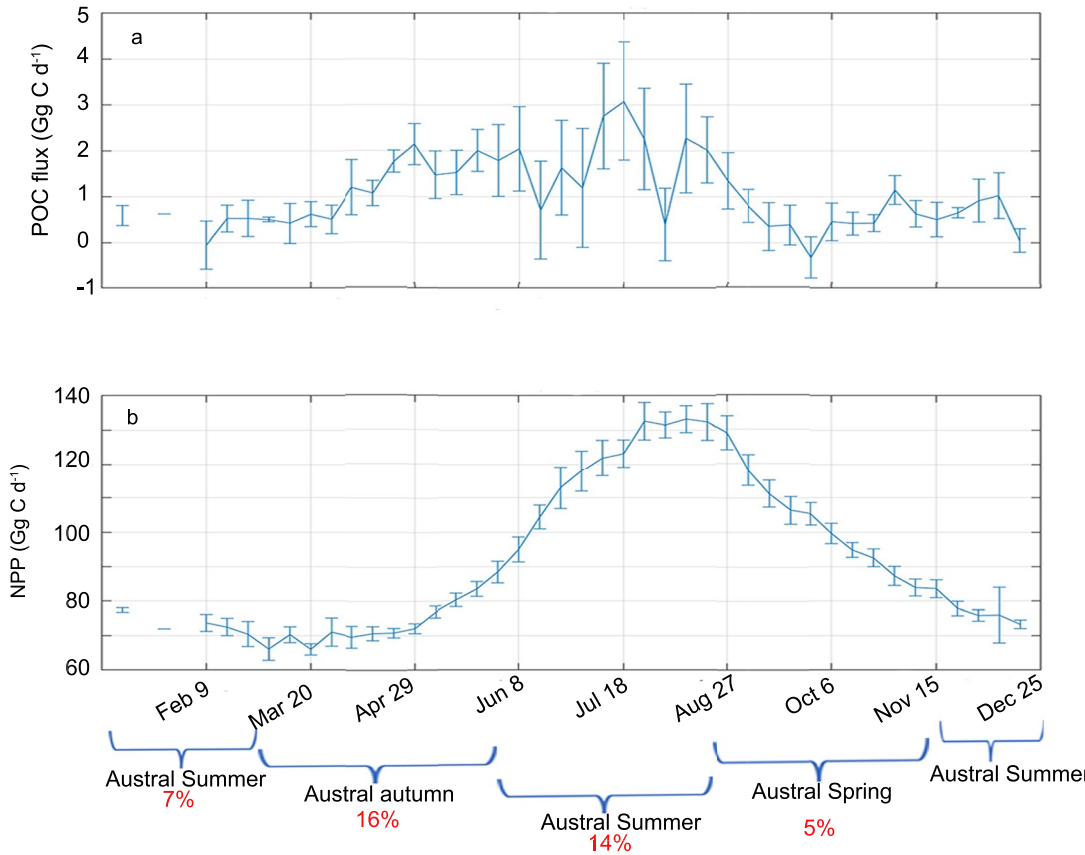

Figure 8. (a) Climatological particulate organic carbon (POC) fluxes calculated from 2003 to 2016 climatological. (b) The climatological trend of net primary productivity (NPP).

the euphotic zone) although with substantial uncertainty. This suggests that other, either physical or biological processes, are primarily responsible for supporting new production in this region. Notably, the three most likely mechanisms of nitrogen transport into the Argo Basin (vertical mixing and/or upwelling of nitrate, lateral transport, and nitrogen fixation) might be expected to respond to climate change with commensurately different ecosystem impacts. Increased surface warming is expected to increase stratification, thus decreasing vertical nutrient introduction, and decreasing primary production (Behrenfeld et al., 2006; Fu et al., 2016). In contrast, increases in differential heating might lead to increased wind speeds and commensurately faster ocean currents and greater lateral transport. The response of marine nitrogen fixation to climate change, which would affect the primary productivity in this region, is uncertain. This is mainly because increased stratification is likely to lead to decreased phosphate supply (necessary for nitrogen fixation), while increased temperatures and an ecological shift from non-diazotrophic phytoplankton to diazotrophs may lead to increased nitrogen fixation rates (Bopp et al., 2022; Wrightson & Tagliabue, 2020).

Our uncertainty in the magnitude of new production supported by lateral transport is substantial. Much of this uncertainty derives from two different sources: uncertainty in quantifying subsurface processes and uncertainty in the regional *f*-ratio. These two sources show up in distinctly different places in our uncertainty calculations. The former is reflected in the fact that our estimates of mixed-layer lateral transport are more than a factor of two lower than our estimates of full euphotic-zone lateral transport. Unfortunately, while subsurface lateral transport should be included in any euphotic zone nitrogen budget, subsurface POC concentrations are not observable by satellite (and woefully under-sampled in the region), while subsurface currents are not available from the GlobCurrent product. Fruitful future progress could be made using four-dimensional coupled physical-biogeochemical models if care is taken in validating model POC and velocity fields. Uncertainty in the *f*-ratio is reflected in the large 95% confidence values for our estimates of lateral POC supply (i.e., 1.9%–61% for mixed-layer transport, 4.6 - >100% for euphotic-zone transport). *f*-ratios are highly variable in the world ocean

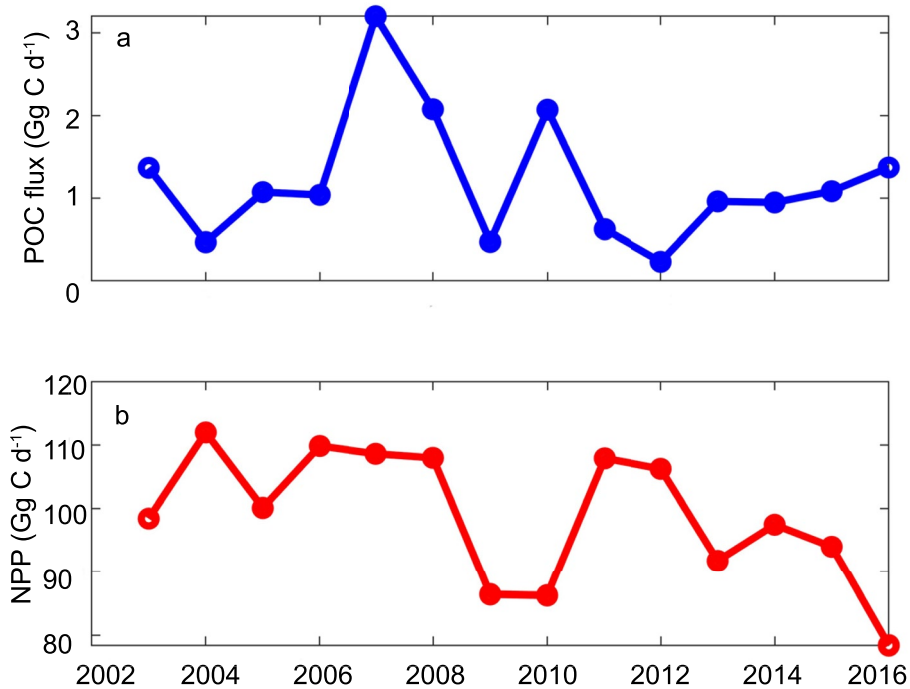

Figure 9. Interannual variability of annual averages from 2003 to 2016. (a) Blue line shows particulate organic carbon flux (Gg C d^{-1}). (b) The red line shows the rate of net primary productivity (Gg C d^{-1}).

(Dugdale & Goering, 1967; Harrison et al., 1993; Laws et al., 2011, p. 201; Sambrotto, 2001). More accurately constraining this term will thus require sampling of nitrate and ammonium uptake rates (or nitrogen export), given the mass-balance constrained equivalence of new production and export (Eppley & Peterson, 1979) in the Argo Basin. An additional source of uncertainty not previously mentioned is related to the C:N stoichiometry of phytoplankton and organic matter. Equations 6 and 7 implicitly assume that the C:N stoichiometry of POM

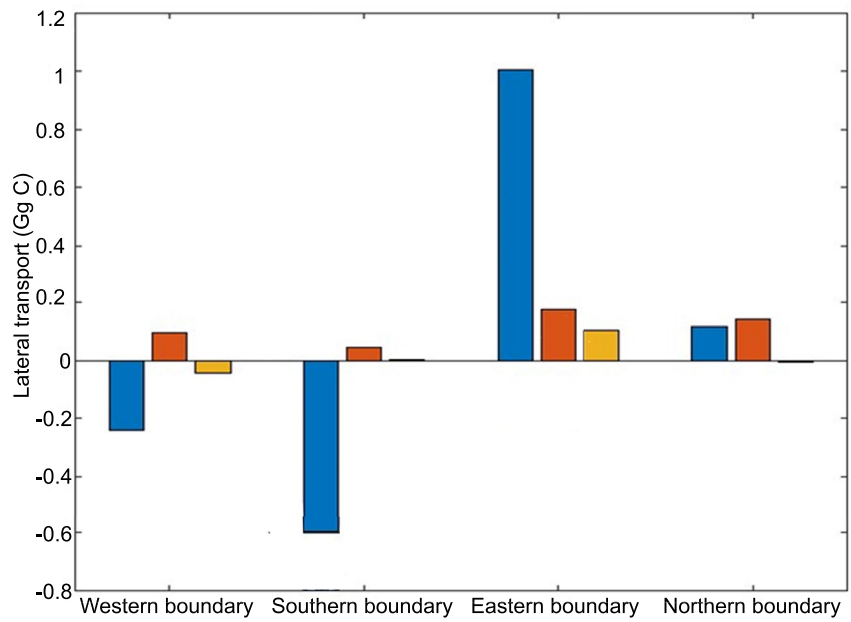

Figure 10. (a) Bar chart showing the lateral transport of particulate organic carbon due to mean flow, transient eddies, and persistent eddies through the four boundaries, positive values indicate influx while negative values indicate outflow.

entering the Argo Basin is equal to the C:N stoichiometry of phytoplankton organic matter production within the region. If suspended POM advected into this region has a different C:N ratio than active phytoplankton growth our estimates of the proportion of new nitrogen derived from lateral transport would need to be revised. Additionally, NPP measurements (i.e., the VGPM-satellite product used herein) do not account for dissolved organic matter released by phytoplankton, which would suggest that our estimates of fraction of NPP supported might need to be revised downward accordingly.

3.6. Mesoscale Eddies

An additional important result of our study is the fact that approximately half of lateral transport is attributable to transient eddies (i.e., mesoscale circulation, since the GlobCurrent product is mostly too coarse to resolve submesoscale features). Mesoscale features have been shown to have substantial biogeochemical impacts as sites of enhanced nutrient supply (Li et al., 2012; McGillicuddy et al., 1998), productivity (Barone et al., 2022; Landry et al., 2008; Oschlies & Garçon, 1998), sinking carbon flux (Benitez-Nelson et al., 2007; Stukel et al., 2017), and organic matter subduction (Omand et al., 2015; Stukel et al., 2017). Mesoscale fronts, eddies, and filaments are also sites of enhanced plankton and fish biomass (Ohman et al., 2012; Schmid et al., 2020; Stukel et al., 2017) and may be important for larval fish survival (Bakun, 2006; Domingues et al., 2016; Shropshire et al., 2022).

Recent results, however, highlight the complex and varied responses of plankton ecosystems to meso- and submesoscale eddies. Autonomous floats have ascertained subsurface phytoplankton responses that are not observable by satellites (Xiu & Chai, 2020). Use of towed imaging platforms have noted fine-scale predator-prey covariances within an eddy (Schmid et al., 2020). Convective mixing within mesoscale eddies can also allow sustained phytoplankton production during transition seasons (Smitha et al., 2022). Waga et al. (2019) have hypothesized that, globally, the responses of phytoplankton size structure to mesoscale eddies varies between oligotrophic and eutrophic regions. Focusing only on regions near our study site: cold-core areas are sites of enhanced productivity (mainly by diatoms) along the Eastern Australian coast (Firme et al., 2023), while eddies seemingly had little impact on phytoplankton production in the *Prochlorococcus*-dominated Philippine Sea (Yun et al., 2020). Results from the Eastern Australian coast also showed entrainment of coastal larval fish into a frontal cyclonic eddy (Garcia et al., 2022). Our results support the importance of mesoscale features in laterally supplying nitrogen-limited offshore regions with critical nutrients (Kelly et al., 2021). Such processes may be important for many oceanographic regions influenced by highly productive upwelled waters such as the California Current Ecosystem (Amos et al., 2019; Chenillat et al., 2015; Nagai et al., 2015), Coast of Chile (Wang et al., 2018) and GoM (Kelly et al., 2021).

3.7. Potential Sources of Laterally Advected POC in the Basin

An example of mesoscale features supporting lateral advection is shown for the year 2007 (Figure 11). High POM water likely originated from upwelling in several locations including the Timor coast, Lombok Strait, and the Australian coast (Figures 1 and 11). We observed a spread of northwest Australian coastal wasters into the oligotrophic region during austral winter; this spread started around June and grew stronger by July (Figures 11e and 11f). A spiral formation of enhanced POC concentrations during this period suggests an eddy trapping in nutrient-rich waters that can sustain higher biomass (Figure 11g). Eddies forming in coastal areas can trap nutrients and transport nutrients and biomass from coastal waters to offshore regions (Amos et al., 2019; Castelao et al., 2021; Nagai et al., 2015; Wang et al., 2018). The productivity of the coastal waters around the Argo Basin during winter may be due to monsoonal activities, with additional contributions from the ITF, which brings in thermocline waters with high nitrate when it passes through the Timor route that can subsequently be upwelled in coastal regions (Ayers et al., 2014). The latter process could be the reason we observed significant POC flux through the northeastern boundary (Figure 11e), coming from Timor coastal waters. Lastly, we observed another flow of POC through the northern boundary of the region around May (Figure 11d). Valsala and Ikeda (2007) showed that the ITF undergoes strong mixing once it enters the Indian Ocean. This flux might be caused by ITF waters that could be mixed or upwelled during this upwelling process, since Ombai is one of the ITF routes into the Indian Ocean, transporting upwelled productive coastal waters of Ombai. However, the eastward flow of POC through the northern region could also be from upwelled waters by currents in the Somali region and laterally advected to this oligotrophic region by the Southern Java Current (SJC). This was suggested by Valsala and Ikeda's (2007) observation that ITF waters reroute through upwelling in the Somali region and

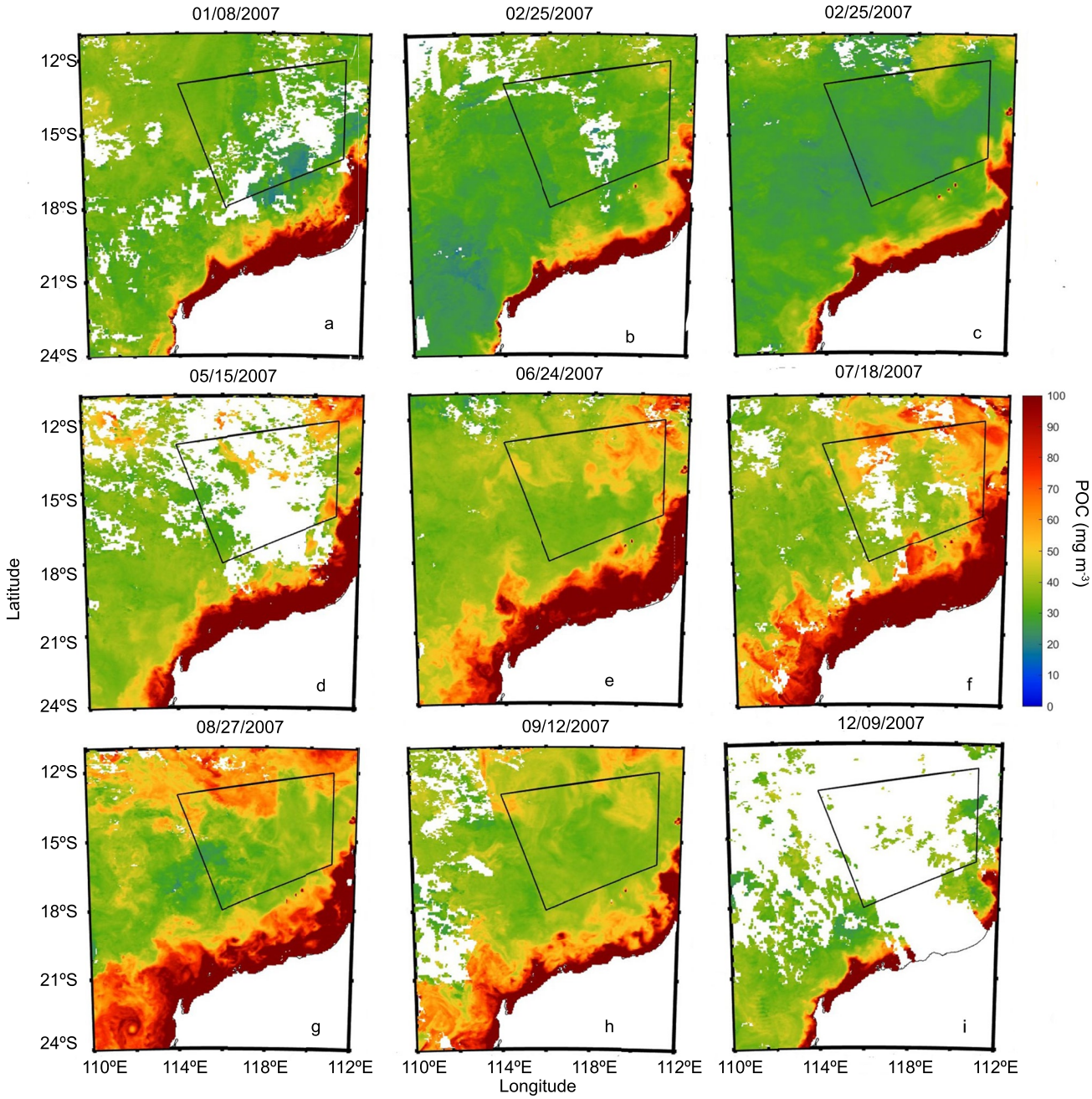

Figure 11. Eight days averaged snapshots of particulate organic carbon (POC) estimates for 2007, from NASA Aqua satellite product data. The boxed area represents the study region.

spread nutrient-rich waters throughout the northern Indian Ocean, with a long residence time of at least 20 yr. The seasonality of the Somali Current is vital to this spread during the Indian summer monsoon from April to October. This spread is likely the reason we also observed a high POC flux during the austral winter (by May) through the northern boundary into our study region. The western boundary does not seem to contribute much POC to the region because this boundary is not surrounded by coastal waters. In addition, a general westward mean flow was observed in this region. Entrainment from productive coastal waters, upwelled ITF waters from outside the region, and transport from the Somali region due to the SJC are possible sources of particulate organic matter that flow into this oligotrophic region, thereby increasing its NPP and supporting the ecosystem, especially during winter.

Our results highlight the importance of interdisciplinary and integrative use of oceanographic and meteorological tools for constraining biogeochemical fluxes. Among still unresolved issues, it is not clear whether the laterally transported organic matter was originally supported by nutrients from the coast of Western Australia or coasts of Islands close to the region, ITF transport of waters from the Pacific Ocean, upwelling associated with these coasts, or from a combination of these. However, our results suggest that lateral advection is less important to the production of this region's ecosystem than in the GoM, although the noted high uncertainty certainly justifies future research.

4. Conclusion

The transport of nitrogen into oligotrophic ecosystems is important for sustained ecosystem productivity. Our study of the oligotrophic Argo Basin suggests that the majority of nitrogen that supports new production in this region is not laterally advected and is more likely to enter the ecosystem as locally upwelled nitrate or through nitrogen fixation. However, substantial uncertainty is clear in our estimates and results primarily from uncertainty in the regional *f*-ratio and an inability to constrain subsurface POM concentrations and horizontal velocities. Lateral introduction of POM primarily occurs through the northern and, especially, eastern boundaries, highlighting the importance of waters of potential ITF origin to the Argo Basin ecosystem. Our results also show that approximately half of all lateral transport results from transient eddies, which likely play an important role across trophic levels. Future advances will require a better understanding of factors that affect the dynamics in this region to quantify other sources of new production supporting the Argo Basin. Future studies could also track eddies in the region, to be certain that organic matter laterally advected through eddies is sourced from the coastal waters as previous works have shown in other regions. Our results can be used to inform predictions and models that simulate the responses of oligotrophic systems to future change and help to better understand the unique Argo Basin ecosystem and decision-making processes to improve management of economically important fishes that spawn within.

Data Availability Statement

Observations are available at https://oceancolor.gsfc.nasa.gov/l3/ (satellite derived particulate organic carbon, 8-day averaged, 4 km resolution), http://tds0.ifremer.fr/thredds/ncss/GLOBCURRENT-L4-CUREUL_15M-ALT_SUM-V03.0/dataset.html (surface currents), https://www.nodc.noaa.gov/OC5/WOA94/mix.html (mixed layer depth), http://orca.science.oregonstate.edu/1080.by.2160.monthly.hdf.vgpm.m.chl.m.sst.php (net primary productivity).

Acknowledgments
A big thank you to our many colleagues at COAPS and collaborators in the BLOOFINZ-IO research project and to the captain and crew members of the *R/V Roger Revelle*. The authors would like to thank NASA, NOAA, and ESA for the distribution of data products. This study was supported by National Science Foundation biological oceanography grants OCE-1851347 to M.R.S. and S.A.K. and OCE-1851558 to M.R.L. and by a fellowship from the Jack Winchester Fund at FSU. This study was a part of project EP-46 of the 2nd International Indian Ocean Expedition (IIOE-2). Sampling in the Argo-Rowley Terrace Marine Park was done under Australian Government permit AU-COM2021-520 and permit PA2021-00062-1 issued by the Director of National Parks, Australia.

References

Amos, C. M., Castelao, R. M., & Medeiros, P. M. (2019). Offshore transport of particulate organic carbon in the California Current System by mesoscale eddies. *Nature Communications*, *10*(1), 4940. https://doi.org/10.1038/s41467-019-12783-5

Ayers, J. M., Strutton, P. G., Coles, V. J., Hood, R. R., & Matear, R. J. (2014). Indonesian throughflow nutrient fluxes and their potential impact on the Indian Ocean productivity. *Geophysical Research Letters*, *8*(14), 5060–5067. https://doi.org/10.1002/2014GL060593

Azam, F., Fenchel, T., Field, J. G., Gray, J. S., Meyer-Reil, L. A., & Thingstad, F. (1983). The ecological role of water-column microbes in the sea. *Marine Ecology Progress Series*, *10*(3), 257–263. https://doi.org/10.7208/chicago/9780226125534-024

Bakun, A. (2006). Fronts and eddies as key structures in the habitat of marine fish larvae: Opportunity, adaptive response, and competitive advantage. *Scientia Marina*, *70*(S2), 105–122. https://doi.org/10.3989/scimar.2006.70s2105

Barkan, R., McWilliams, J. C., Shchepetkin, A. F., Molemaker, M. J., Renault, L., Bracco, A., & Choi, J. (2017). Submesoscale dynamics in the northern Gulf of Mexico. Part I: Regional and seasonal characterization and the role of river outflow. *Journal of Physical Oceanography*, *47*(9), 2325–2346. https://doi.org/10.1175/JPO-D-17-0035.1

Barone, B., Church, M. J., Dugenne, M., Hawco, N. J., Jahn, O., White, A. E., et al. (2022). Biogeochemical dynamics in adjacent mesoscale eddies of opposite polarity. *Global Biogeochemical Cycles*, *36*(2), e2021GB007115. https://doi.org/10.1029/2021gb007115

Behrenfeld, M. J., & Falkowski, P. G. (1997). Photosynthetic rates derived from satellite-based chlorophyll concentration. *Limnology and Oceanography*, *42*(1), 1–20. https://doi.org/10.4319/lo.1997.42.1.0001

Behrenfeld, M. J., O'Malley, R. T., Siegel, D. A., McClain, C. R., Sarmiento, J. L., Feldman, G. C., et al. (2006). Climate-driven trends in contemporary ocean productivity [Dataset]. *Nature*, *444*(7120), 752–755. https://doi.org/10.1038/nature05317

Benitez-Nelson, C. R., Bidigare, R. R., Dickey, T. D., Landry, M. R., Leonard, C. L., Brown, S. L., et al. (2007). Mesoscale eddies drive increased silica export in the subtropical Pacific Ocean. *Science*, *316*(5827), 1017–1021. https://doi.org/10.1126/science.1136221

Bonjean, F., & Lagerloef, G. S. E. (2002). Diagnostic model and analysis of the surface currents in the tropical Pacific Ocean. *Journal of Physical Oceanography*, *32*(10), 2938–2954. https://doi.org/10.1175/1520-0485

Bopp, L., Aumont, O., Kwiatkowski, L., Clerc, C., Dupont, L., Ethé, C., et al. (2022). Diazotrophy as a key driver of the response of marine net primary productivity to climate change. *Biogeosciences*, *19*(17), 4267–4285. https://doi.org/10.5194/bg-19-4267-2022

Cancet, M., Griffin, D., Cahill, M., Chapron, B., Johannessen, J., & Donlon, C. (2019). Evaluation of GlobCurrent surface ocean current products: A case study in Australia. *Remote Sensing of Environment*, *220*, 71–93. https://doi.org/10.1016/j.rse.2018.10.029

Castelao, R. M., Dinniman, M. S., Amos, C. M., Klinck, J. M., & Medeiros, P. M. (2021). Eddy-driven transport of particulate organic carbon-rich coastal water off the west Antarctic Peninsula. *Journal of Geophysical Research: Oceans*, *126*(3). https://doi.org/10.1029/2020JC016791

Chabert, P., d'Ovidio, F., Echevin, V., Stukel, M. R., & Ohman, M. D. (2021). Cross-shore flow and implications for carbon export in the California current ecosystem: A Lagrangian analysis. *Journal of Geophysical Research: Oceans*, *126*(2). https://doi.org/10.1029/2020JC016611(2002)032<2938:DMAAOT>2.0.CO;2

Chenillat, F., Franks, P. J. S., Rivière, P., Capet, X., Grima, N., & Blanke, B. (2015). Plankton dynamics in a cyclonic eddy in the Southern California current system. *Journal of Geophysical Research: Oceans*, *120*(8), 5566–5588. https://doi.org/10.1002/2015JC010826

Domingues, R., Goni, G., Bringas, F., Muhling, B., Lindo-Atichati, D., & Walter, J. (2016). Variability of preferred environmental conditions for Atlantic bluefin tuna (*Thunnus thynnus*) larvae in the Gulf of Mexico during 1993–2011. *Fisheries Oceanography*, *25*(3), 320–336. https://doi.org/10.1111/fog.12152

Duce, R. A., LaRoche, J., Altieri, K., Arrigo, K. R., Baker, A. R., Capone, D. G., et al. (2008). Impacts of atmospheric anthropogenic nitrogen on the open ocean. *Science*, *320*(5878), 893–897. https://doi.org/10.1126/science.1150369

Dugdale, R. C., & Goering, J. J. (1967). Uptake of new and regenerated forms of nitrogen in primary productivity1: Uptake of nitrogen in primary productivity. *Limnology & Oceanography*, *12*(2), 196–206. https://doi.org/10.4319/lo.1967.12.2.0196

Eppley, R. W., & Peterson, B. J. (1979). Particulate organic matter flux and planktonic new production in the deep ocean. *Nature*, *282*(5740), 677–680. https://doi.org/10.1038/282677a0

Estapa, M. L., Siegel, D. A., Buesseler, K. O., Stanley, R. H. R., Lomas, M. W., & Nelson, N. B. (2015). Decoupling of net community and export production on submesoscales in the Sargasso Sea. *Global Biogeochemical Cycles*, *29*(8), 1266–1282. https://doi.org/10.1002/2014GB004913

Evers-King, H., Martinez-Vicente, V., Brewin, R. J. W., Dall'Olmo, G., Hickman, A. E., Jackson, T., et al. (2017). Validation and intercomparison of ocean color algorithms for estimating particulate organic carbon in the oceans. *Frontiers in Marine Science*, *4*. https://doi.org/10.3389/fmars.2017.00251

Fennel, K., & Laurent, A. (2018). N and P as ultimate and proximate limiting nutrients in the northern Gulf of Mexico: Implications for hypoxia reduction strategies. *Biogeosciences*, *15*(10), 3121–3131. https://doi.org/10.5194/bg-15-3121-2018

Firme, G. F., Hughes, D. J., Laiolo, L., Roughan, M., Suthers, I. M., & Doblin, M. A. (2023). Contrasting phytoplankton composition and primary productivity in multiple mesoscale eddies along the East Australian coast. *Deep Sea Research Part I: Oceanographic Research Papers*, *193*, 103952. https://doi.org/10.1016/j.dsr.2022.103952

Fu, W., Randerson, J. T., & Moore, J. K. (2016). Climate change impacts on net primary production (NPP) and export production (EP) regulated by increasing stratification and phytoplankton community structure in the CMIP5 models. *Biogeosciences*, *13*(18), 5151–5170. https://doi.org/10.5194/bg-13-5151-2016

Garcia, V., Schilling, H. T., Cruz, D. O., Hawes, S. M., Everett, J. D., Roughan, M., et al. (2022). Entrainment and development of larval fish assemblages in two contrasting cold core eddies of the East Australian Current system. *Marine Ecology Progress Series*, *685*, 1–18. https://doi.org/10.3354/meps13982

Gerard, T., Lamkin, J. T., Kelly, T. B., Knapp, A. N., Laiz-Carrión, R., Malca, E., et al. (2022). Bluefin larvae in oligotrophic ocean foodwebs, investigations of nutrients to zooplankton: Overview of the BLOOFINZ-Gulf of Mexico program. *Journal of Plankton Research*, *44*(5), 600–617. https://doi.org/10.1093/plankt/fbac038

Granéli, E., Carlsson, P., & Legrand, C. (1999). The role of C, N, and P in dissolved and particulate organic matter as a nutrient source for phytoplankton growth, including toxic species. *Aquatic Ecology*, *33*(1), 17–27. https://doi.org/10.1023/a:1009925515059

Harrison, W. G., Head, E. J. H., Horne, E. P. W., Irwin, B., Li, W. K. W., Longhurst, A. R., et al. (1993). The western North Atlantic bloom experiment. *Deep Sea Research Part II: Topical Studies in Oceanography*, *40*(1–2), 279–305. https://doi.org/10.1016/0967-0645(93)90018-I

Kelly, T. B., Knapp, A. N., Landry, M. R., Selph, K. E., Shropshire, T. A., Thomas, R. K., & Stukel, M. R. (2021). Lateral advection supports nitrogen export in the oligotrophic open-ocean Gulf of Mexico. *Nature Communications*, *12*(1), 3325. https://doi.org/10.1038/s41467-021-23678-9

Kranz, S. A., Wang, S., Kelly, T. B., Stukel, M. R., Goericke, R., Landry, M. R., & Cassar, N. (2020). Lagrangian studies of marine production: A multimethod assessment of productivity relationships in the California current ecosystem upwelling region. *Journal of Geophysical Research: Oceans*, *125*(6), e2019JC015984. https://doi.org/10.1029/2019JC015984

Landry, M. R., Brown, S. L., Rii, Y. M., Selph, K. E., Bidigare, R. R., Yang, E. J., & Simmons, M. P. (2008). Depth-stratified phytoplankton dynamics in Cyclone Opal, a subtropical mesoscale eddy. *Deep Sea Research Part II: Topical Studies in Oceanography*, *55*(10–13), 1348–1359. https://doi.org/10.1016/j.dsr2.2008.02.001

Landry, M. R., Ohman, M. D., Goericke, R., Stukel, M. R., & Tsyrklevich, K. (2009). Lagrangian studies of phytoplankton growth and grazing relationships in a coastal upwelling ecosystem off Southern California. *Progress in Oceanography*, *83*(1–4), 208–216. https://doi.org/10.1016/j.pocean.2009.07.026

Laws, E. A., D'Sa, E., & Naik, P. (2011). Simple equations to estimate ratios of new or export production to total production from satellite-derived estimates of sea surface temperature and primary production. *Limnology and Oceanography: Methods*, *9*(12), 593–601. https://doi.org/10.4319/lom.2011.9.593

Li, Q. P., Franks, P. J. S., Ohman, M. D., & Landry, M. R. (2012). Enhanced nitrate fluxes and biological processes at a frontal zone in the southern California current system. *Journal of Plankton Research*, *34*(9), 790–801. https://doi.org/10.1093/plankt/fbs006

Lipschultz, F. (2001). A time-series assessment of the nitrogen cycle at BATS. *Deep Sea Research Part II: Topical Studies in Oceanography*, *48*(8–9), 1897–1924. https://doi.org/10.1016/S0967-0645(00)00168-5

Lorenz, E. N. (1967). *The nature and theory of the general circulation of the atmosphere (Part 2)* (Vol. 218, p. 161). World Meteorological Organization. Retrieved from https://eapsweb.mit.edu/sites/default/files/General_Circ_WMO_1967_Part2.pdf

McGillicuddy, D. J., Robinson, A. R., Siegel, D. A., Jannasch, H. W., Johnson, R., Dickey, T. D., et al. (1998). Influence of mesoscale eddies on new production in the Sargasso Sea. *Nature*, *394*(6690), 263–266. https://doi.org/10.1038/28367

Monterey, G. I., & Levitus, S. (1997). Seasonal variability of mixed layer depth for the world ocean. NOAA NESDIS Atlas 14 [Dataset]. National Oceanic and Atmospheric Administration, Silver Spring, MD. https://repository.library.noaa.gov/view/noaa/49153/noaa_49153_DS1.pdf

Muhling, B. A., Lamkin, J. T., Alemany, F., García, A., Farley, J., Ingram, G. W., et al. (2017). Reproduction and larval biology in tunas, and the importance of restricted area spawning grounds. *Reviews in Fish Biology and Fisheries*, *27*(4), 697–732. https://doi.org/10.1007/s11160-017-9471-4

Nagai, T., Gruber, N., Frenzel, H., Lachkar, Z., McWilliams, J. C., & Plattner, G.-K. (2015). The dominant role of eddies and filaments in the offshore transport of carbon and nutrients in the California Current System. *Journal of Geophysical Research: Oceans*, *120*(8), 5318–5341. https://doi.org/10.1002/2015JC010889

Nieblas, A.-E., Demarcq, H., Drushka, K., Sloyan, B., & Bonhommeau, S. (2014). Front variability and surface ocean features of the presumed southern bluefin tuna spawning grounds in the tropical southeast Indian Ocean. *Deep Sea Research Part II: Topical Studies in Oceanography*, *107*, 64–76. https://doi.org/10.1016/j.dsr2.2013.11.007

Ohman, M. D., Powell, J. R., Picheral, M., & Jensen, D. W. (2012). Mesozooplankton and particulate matter responses to a deep-water frontal system in the southern California Current System. *Journal of Plankton Research*, *34*(9), 815–827. https://doi.org/10.1093/plankt/fbs028

Omand, M. M., D'Asaro, E. A., Lee, C. M., Perry, M. J., Briggs, N., Cetinić, I., & Mahadevan, A. (2015). Eddy-driven subduction exports particulate organic carbon from the spring bloom. *Science*, *348*(6231), 222–225. https://doi.org/10.1126/science.1260062

Oschlies, A., & Garçon, V. (1998). Eddy-induced enhancement of primary production in a model of the North Atlantic Ocean. *Nature*, *394*(6690), 266–269. https://doi.org/10.1038/28373

Plattner, G.-K., Gruber, N., Frenzel, H., & McWilliams, J. C. (2005). Decoupling marine export production from new production. *Geophysical Research Letters*, *32*(11), L11612. https://doi.org/10.1029/2005GL022660

Rio, M.-H., Mulet, S., & Picot, N. (2014). Beyond GOCE for the ocean circulation estimate: Synergetic use of altimetry, gravimetry, and in situ data provides new insight into geostrophic and Ekman currents [Dataset]. *Geophysical Research Letters*, *41*(24), 8918–8925. https://doi.org/10.1002/2014GL061773

Rooker, J. R., Alvarado Bremer, J. R., Block, B. A., Dewar, H., de Metrio, G., Corriero, A., et al. (2007). Life history and stock structure of Atlantic bluefin tuna (*Thunnus thynnus*). *Reviews in Fisheries Science*, *15*(4), 265–310. https://doi.org/10.1080/10641260701484135

Sambrotto, R. N. (2001). Nitrogen production in the northern Arabian Sea during the spring intermonsoon and Southwest Monsoon seasons. *Deep Sea Research Part II: Topical Studies in Oceanography*, *48*(6–7), 1173–1198. https://doi.org/10.1016/S0967-0645(00)00135-1

Schmid, M. S., Cowen, R. K., Robinson, K., Luo, J. Y., Briseño-Avena, C., & Sponaugle, S. (2020). Prey and predator overlap at the edge of a mesoscale eddy: Fine-scale, in situ distributions to inform our understanding of oceanographic processes. *Scientific Reports*, *10*(1), 921. https://doi.org/10.1038/s41598-020-57879-x

Shiroza, A., Malca, E., Lamkin, J. T., Gerard, T., Landry, M. R., Stukel, M. R., et al. (2022). Active prey selection in developing larvae of Atlantic bluefin tuna (*Thunnus thynnus*) in spawning grounds of the Gulf of Mexico. *Journal of Plankton Research*, *44*(5), 728–746. https://doi.org/10.1093/plankt/fbab020

Shropshire, T. A., Morey, S. L., Chassignet, E. P., Bozec, A., Coles, V. J., Landry, M. R., et al. (2020). Quantifying spatiotemporal variability in zooplankton dynamics in the Gulf of Mexico with a physical-biogeochemical model. *Biogeosciences*, *17*(13), 3385–3407. https://doi.org/10.5194/bg-17-3385-2020

Shropshire, T. A., Morey, S. L., Chassignet, E. P., Karnauskas, M., Coles, V. J., Malca, E., et al. (2022). Trade-offs between risks of predation and starvation in larvae make the shelf break an optimal spawning location for Atlantic bluefin tuna. *Journal of Plankton Research*, *44*(5), 782–798. https://doi.org/10.1093/plankt/fbab041

Smitha, B. R. S., Sanjeevan, V., Padmakumar, K., Hussain, M. S., Salini, T., & Lix, J. (2022). Role of mesoscale eddies in the sustenance of high biological productivity in North Eastern Arabian Sea during the winter-spring transition period. *Science of the Total Environment*, *809*, 151173. https://doi.org/10.1016/j.scitotenv.2021.151173

Steinberg, D. K., & Landry, M. R. (2017). Zooplankton and the ocean carbon cycle. *Annual Review of Marine Science*, *9*(1), 413–444. https://doi.org/10.1146/annurev-marine-010814-015924

Stoecker, D. K., Hansen, P. J., Caron, D. A., & Mitra, A. (2017). Mixotrophy in the marine plankton. *Annual Review of Marine Science*, *9*(1), 311–335. https://doi.org/10.1146/annurev-marine-010816-060617

Stramski, D., Reynolds, R. A., Babin, M., Kaczmarek, S., Lewis, M. R., Rottgers, R., et al. (2008). Relationships between the surface concentration of particulate organic carbon and optical properties in the eastern South Pacific and eastern Atlantic Oceans [Dataset]. *Biogeosciences*, *5*(1), 171–201. https://doi.org/10.5194/bg-5-171-2008

Stukel, M. R., Aluwihare, L. I., Barbeau, K. A., Chekalyuk, A. M., Goericke, R., Miller, A. J., et al. (2017). Mesoscale ocean fronts enhance carbon export due to gravitational sinking and subduction. *Proceedings of the National Academy of Sciences*, *114*(6), 1252–1257. https://doi.org/10.1073/pnas.1609435114

Sudre, J., Maes, C., & Garçon, V. (2013). On the global estimates of geostrophic and Ekman surface currents. *Limnology and Oceanography: Fluids and Environments*, *3*(1), 1–20. https://doi.org/10.1215/21573689-2071927

Suthers, I. M., Schaeffer, A., Archer, M., Roughan, M., Griffin, D. A., Chapman, C. C., et al. (2023). Frontal eddies provide an oceanographic triad for favorable larval fish habitat. *Limnology & Oceanography*. https://doi.org/10.1002/lno.12326

Tomczak, M., & Godfrey, J. S. (2003). *Regional oceanography: An introduction*. Daya Books.

Valsala, V. K., & Ikeda, M. (2007). Pathways and effects of the Indonesian throughflow water in the Indian Ocean using particle trajectory and tracers in an OGCM. *Journal of Climate*, *20*(13), 2994–3017. https://doi.org/10.1175/JCLI4167.1

Waga, H., Hirawake, T., & Ueno, H. (2019). Impacts of mesoscale eddies on phytoplankton size structure. *Geophysical Research Letters*, *46*(22), 13191–13198. https://doi.org/10.1029/2019gl085150

Waite, A. M., Beckley, L. E., Guidi, L., Landrum, J. P., Holliday, D., Montoya, J., et al. (2016). Cross-shelf transport, oxygen depletion, and nitrate release within a forming mesoscale eddy in the eastern Indian Ocean: Oxygen, nitrogen, and particles in a forming eddy. *Limnology & Oceanography*, *61*(1), 103–121. https://doi.org/10.1002/lno.10218

Wang, Y., Zhang, H.-R., Chai, F., & Yuan, Y. (2018). Impact of mesoscale eddies on chlorophyll variability off the coast of Chile. *PLoS One*, *13*(9), e0203598. https://doi.org/10.1371/journal.pone.0203598

Wrightson, L., & Tagliabue, A. (2020). Quantifying the impact of climate change on marine diazotrophy: Insights from Earth system models. *Frontiers in Marine Science*, *7*, 635. https://doi.org/10.3389/fmars.2020.00635

Xiu, P., & Chai, F. (2020). Eddies affect subsurface phytoplankton and oxygen distributions in the North Pacific Subtropical Gyre. *Geophysical Research Letters*, *47*(15), e2020GL087037. https://doi.org/10.1029/2020gl087037

Yelton, A. P., Acinas, S. G., Sunagawa, S., Bork, P., Pedrós-Alió, C., & Chisholm, S. W. (2016). Global genetic capacity for mixotrophy in marine picocyanobacteria. *The ISME Journal*, *10*(12), 2946–2957. https://doi.org/10.1038/ismej.2016.64

Yingling, N., Kelly, T. B., Shropshire, T. A., Landry, M. R., Selph, K. E., Knapp, A. N., et al. (2022). Taxon-specific phytoplankton growth, nutrient utilization, and light limitation in the oligotrophic Gulf of Mexico. *Journal of Plankton Research*, *44*(5), 656–676. https://doi.org/10.1093/plankt/fbab028

Yun, M. S., Kim, Y., Jeong, Y., Joo, H. T., Jo, Y. H., Lee, C. H., et al. (2020). Weak response of biological productivity and community structure of phytoplankton to mesoscale eddies in the oligotrophic Philippine Sea. *Journal of Geophysical Research: Oceans*, *125*(12), e2020JC016436. https://doi.org/10.1029/2020JC016436